# Glaucoma Detection using Tetragonal Local Octa Patterns and SVM from Retinal Images

Marriam Nawaz, Tahira Nazir, and Momina Masood
Department of Computer Science, University of Engineering and Technology, Pakistan

**Abstract:** *Glaucoma is a fatal disease caused by the imbalance of intraocular pressure inside the eye which can result in lifetime blindness of the victim. Efficient screening systems require experts to manually analyze the images to recognize the disease. However, the challenging nature of the screening method and lack of trained human resources, effective screening-oriented treatment is an expensive task. The automated systems are trying to cope with these challenges; however, these methods are not generalized well to large datasets and real-world scenarios. Therefore, we have introduced an automated glaucoma detection system by employing the concept of the Content-Based Image Retrieval (CBIR) domain. The Tetragonal Local Octa Pattern (T-LOP) is used for features computation which is employed to train the SVM classifier to show the technique significance. We have evaluated our method over challenging datasets namely, Online Retinal Fundus Image (ORIGA) and High-Resolution Fundus (HRF). Both the qualitative and quantitative results show that our technique outperforms the latest approaches due to the effective localization power of T-LOP as it computes the anatomy independent features and ability of Support Vector Machine (SVM) to deal with over-fitted training data. Therefore, the presented technique can play an important role in the automated recognition of glaucoma lesions and can be applied to other medical diseases as well.*

**Keywords:** *Retinal images, glaucoma, SVM, classification.*

*Received April 28, 2020; accepted November 24, 2020*
*https://doi.org/10.34028/iajit/18/5/8*

## 1. Introduction

Glaucoma is a combination of eye diseases that causes injury in the optic nerve because of an abnormal Intraocular Pressure (IOP) in the eye [31]. The main reason for IOP is the imbalance between the amount of produced and drained intraocular fluid of the eye [10] and ultimately causes to damage the nerve fibers. The affected nerve fibers weaken the Retinal Nerve Fiber Layer (RNFL) and produced the enlarged Cup-To-Disc Ratio (CDR) (or "cupping") and Optic Disc (OD) or Optic Nerve Head (ONH) [26]. The IOP can also result in the deterioration of the retinal pigment epithelium named Peripapillary Atrophy (PPA). From research, it has been revealed that an increase in PPA can cause to produce an acceleration in glaucoma [11]. Figure 1 is representing glaucoma affected eye. From the figure, it can be visualized that the intraocular fluid blockage causes to produce the injury of the optic nerve. The size of OD in the glaucoma affected eye is large as compared to the normal eye.

According to recent research, glaucoma is one of the main reasons for blindness and has been predicted to damage the vision of about 80 million people around the globe by 2020 [25]. It results in complete blindness and usually diagnoses at its advanced level. Therefore, it is named the "silent thief of sight" [19]. Although, despite huge advances in the field of medical [2, 13, 18, 27], still the glaucoma is an incurable disease, however, the complete damage to human sight can be prevented by diagnosing it at its earliest stage. According to another research, it is predicted that in 2040, the range of glaucoma affected people will be increased to 111.8 million [30]. The huge increase in the size of glaucomatous cupping will not only put an economic or social burden but will also affect the comfort of the victims [31]. Although, several methods have been proposed to detect Glaucoma at its earliest stage, however, these approaches may not perform well over real-world problems due to the varying properties of glaucomatous region. Therefore, an effective and efficient glaucoma detection system is required to reduce its damage and to save the people from its devastating impacts.


Figure 1. Visual example of a glaucomatous region in a retinal image.

Early and accurate automated detection of glaucoma is still a challenging task due to its texture, size, and subtle border etc. Existing approaches are dependent of manual screening prices which has huge computational complexity. In this paper, we have tried to overcome

these challenges by employing the multi-group recognition concept of Content-Based Image Retrieval (CBIR) with feature extraction. The presented approach is independent of manual grading and efficient in terms of economic cost factor. Our technique follows a two-step process. Initially, keypoints are computed of a given query sample using Tetragonal Local Octa Pattern (T-LOP). Then Support Vector Machine (SVM) classifier is trained on computed features to classify glaucoma into various classes. Secondly, we compute the top neighbourhood of the input sample from the historical fundus images database for determining the informed decision related to prescriptions. To the best of our knowledge, it is the first time in medical history when T-LOP along with the CBIR concept has been utilized for automated glaucoma detection. Our work has the following contributions:

- Accurate and precise detection of glaucoma because of effective localization power of T-LOP as it computes the anatomy independent features.
- Efficient classification of the glaucomatous image because of accuracy and the power of SVM classifier to deal with the over-fitted training data.
- Achieved state-of-the-art performance over glaucoma challenging dataset named "ORIGA".
- Employs the concept of CBIR with glaucoma detection to assist in determining the earlier prescription for victims.

The rest of the paper has the following structure: section 2 presents the related work, while the proposed framework is discussed in detail in section 3. Performance evaluation of our framework is presented in section 4, and finally, section 5 concludes the proposed work.

## 2. Related Work

Early detection of glaucoma lesions can save the individual from complete vision loss. Therefore, researchers have introduced several techniques to efficiently localize and detect glaucoma diseases. Li *et al*. [15] proposed a deep residual neural network (ResNet 101) for the classification of glaucoma from color fundus images. As a pre-processing step, the Hough transform technique is employed to trim ONH (optic nerve head) center from the surrounding region. The proposed model considered the patient's medical history as well to study its influence on the ability to distinguish normal healthy eyes from Glaucomatous Optic Neuropathy (GON) suspected and confirmed eyes. Martins *et al*. [20] developed a model based on GFI-ASPP-Depth architecture for the diagnosis of glaucoma. The proposed approach performs the combined segmentation of both the optic disc and optic cup. For classification different morphological features such as Vertical Cup-To-Disc Ratio (VCDR), CDR, Rim to Disc Area Ratio (RDAR), and Neuro-Retinal Rim (NRR) are calculated.

Hemelings *et al*. [12] proposed a deep learning approach using ResNet-50 encoder for glaucoma classification. Due to the limited amount of availability of labelled training data, transfer learning and active learning are employed to reduce the labelling cost and resulted in improved performance in terms of accuracy, specificity, and sensitivity. Li *et al*. [16] proposed a weakly-supervised attention-based Convolutional Neural Network model (AG-CNN) based on residual networks for the detection of glaucoma. The attention maps are predicted to ignore the redundant regions containing no valuable information and highlight the salient regions i.e., pathological areas which are then used to extract feature maps for localization and classification of glaucoma. Guo *et al*. [9] proposed an automated method to compute the vertical CDR for the diagnosis of glaucoma. The vasculature and disk selective Combination Of Shifted Filter Responses (COSFIRE) filters are first applied to localize the OD then a Generalized Matrix Learning Vector Quantization classifier (GMLVQ) is used to determine the boundary of the optic disc and the cup.

Yu *et al*. [33] proposed a deep learning-based approach for automated segmentation of OD and cup segmentation by modifying the U-net architecture. Using CDR, they achieved an average disc and cup segmentation dice score of 97% and 87% respectively. However, the proposed model is sensitive to the quality of fundus images. In [8] a VGG19 network via transfer learning is used to diagnose glaucoma. Bajwa *et al*. [1] proposed a two-stage framework for glaucoma detection. First, the faster Region-based Convolutional Neural Network (RCNN) extracts the ROI, and the second CNN network classifies it into healthy or glaucoma affected. The proposed approach performs better than existing heuristic localization techniques. However, this approach requires images to be annotated for training.

Zhao *et al*. [35] a weakly-Supervised Multi-Task Learning (WSMTL) framework is developed for the identification of evidence area, OD segmentation, and glaucoma classification simultaneously. A constrained clustering branch network takes an evidence map as input to generate an OD segmentation mask which is then further passed to a fully connected convolutional network to classify the fundus as normal or glaucoma. Liao *et al*. [17] presents a similar work as in proposed [35], the evidence activation maps are generated for accurate diagnosis of glaucoma. A ResNet network with multi-layers average pooling is employed to map between global semantic information and precise localization. The model achieves an Area Under the Curve (AUC) of 0.88 and dice of 0.9 for optic disc segmentation using the ORIGA datasets. Several machine learning and deep learning-based approaches have been employed for the detection of glaucoma [4, 6,

14, 21, 22, 28, 32, 34], however, still, there is room for performance improvement.

## 3. Proposed Methodology

The flow of the proposed work is represented in Figure 2. In our work, glaucoma detection is performed by following a two-way technique. In the first step, the image features are extracted by employing the T-LOP [29] method, which is then used to train the SVM classifier. After model training, a query image is passed to the model to classify as glaucoma affected or not. In the second step, for glaucoma images, we compute the features of the image by computing the query neighbourhood and return the system output. In CBIR the contextual information of the query image is examined to extract the semantically similar images from the large database of images [24].

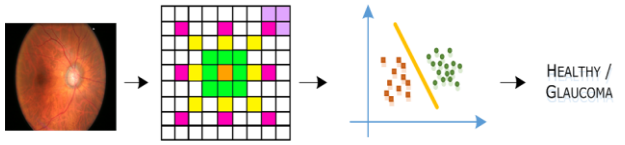


a) Input. b) T-LOP (Feature Extraction). c) SVM (classification). d) Output.

Figure 2. Workflow of Proposed method.

The semantic information of the image is computed by estimating the image intrinsic features or by producing the global image representations [7]. The computed image features are used to measure the similarity with database images and top-matched results are restored. However, the semantic information of digital images is usually concerned with image analysis along with dense objects, complicated backgrounds, and complex overlapping semantics, therefore, the latest techniques of CBIR are employing the supervised learning techniques. So, in modern CBIR approaches, image retrieval is utilized for image classification problems in which the semantic classifiers are defined to compute the semantic information of the images.

The utilization of the concept of employing the semantic classifier of CBIR for glaucoma detection is the main inspiration of our proposed work. In our technique, glaucoma-affected images are detected in the same manner as the semantic response is computed in CBIR systems. In CBIR, the related images are shown as output of the system, while in glaucoma detection systems, the semantic classifier is used to return the relevant historical cases from the image databases which can assist in determining the prescriptions.

- *Input Data*: for the given dataset of images, the glaucoma detection system works by producing the low-level keypoints representation of all input samples and divides the whole image dataset into small image-based $l_j$ (where j=1, 2, 3,…N) named as a Bag Of Images (BOI), which have positive and negative images of glaucoma which are given as follows:

The positive examples are represented by $D_j^+$ and given as in Equation (1):

$$Da_j^+ = (Da/N) \times q \tag{1}$$

Where

$$Da_j{}^+ = \{x_1, x_2, \ldots, x_{Da_l}\} \tag{2}$$

In Equation (1) Da is the total number of examples in the whole dataset, $N$ is the number of subsets, and the value of $q$ can vary from 0 to 1 to show the positive BOI size in jth subset.

While the negative examples are shown by $Da_j^-$ and given as in Equation (3):

$$Da_i{}^- = \{x_1, x_2, \ldots, x_{Da-Da_l} | Da^+ \cap Da_j^- = \emptyset\} \tag{3}$$

Where $x_j$ is representing the total number of features within each BOI. To have an efficient glaucoma screening system, it is very important to have the robust features representation of fundus images in form of feature vectors to ensure precise glaucoma detection.

- Feature extraction: In this paper, we have introduced T-LOP by employing the concept of Local Tetra Patterns (LTrPs) [23] to obtain the discriminative set of features from the fundus images. A detailed description of LBP is given in Appendix A. T-LOP patterns work by utilizing the pixels directions along the horizontal, vertical, and diagonal positions to preserve the patterns of different diagonals to represent the various regions. The novelty of the obtained patterns is that these not only reduces the length of the obtained feature vector but also produces the rotation invariant images. Furthermore, the usage of diagonals of different sizes allows achieving the scale-invariant representation. The key motivation of employing the derivatives along the diagonal direction together with LTrPs is the LTrPs patterns only use the derivates along with the horizontal and vertical directions, however, the fundus images contain the blood vessels with diagonals shapes also. So, LTrPs patterns exhibit lower performance as these patterns are unable to encode the diagonal shaped vessels effectively. So, to cope with the limitations of LTrPs, these patterns are modified by computing the derivatives in four directions, rather than employing only two derivatives. The (n-1)$^{th}$ order derivatives are computed by the T-LOP descriptor along with the following directions: 0°, 45°, 90°, and 135° as mentioned in [20], and the value of the central pixel $g_{cen}$ is calculated by Equation (4):

$$\begin{aligned}
&1.\mathrm{Im}\, g_{0^o}^{N-1}(g_{cen}) \geq 0 \wedge \mathrm{Im}\, g_{90^o}^{N-1}(g_{cen}) \geq 0 \wedge (\mathrm{Im}\, g_{45^o}^{N-1}(g_{cen}) \vee \mathrm{Im}\, g_{135^o}^{N-1}(g_{cen})) \geq 0 \\
&2.\mathrm{Im}\, g_{0^o}^{N-1}(g_{cen}) < 0 \wedge \mathrm{Im}\, g_{90^o}^{N-1}(g_{cen}) \geq 0 \wedge (\mathrm{Im}\, g_{45^o}^{N-1}(g_{cen}) \vee \mathrm{Im}\, g_{135^o}^{N-1}(g_{cen})) \geq 0 \\
&. \\
&. \\
&8.\mathrm{Im}\, g_{0^o}^{N-1}(g_{cen}) \geq 0 \wedge \mathrm{Im}\, g_{90^o}^{N-1}(g_{cen}) < 0 \wedge (\mathrm{Im}\, g_{45^o}^{N-1}(g_{cen}) \vee \mathrm{Im}\, g_{135^o}^{N-1}(g_{cen})) < 0
\end{aligned} \quad (4)$$

After computing the direction of the central pixel, the nth order T-LOPs is given by Equation (5):

$$TLOP_P^N(g_{cen}) = \{ f_6(\mathrm{Im}\, g_D^{'N-1}(g), \mathrm{Im}\, g_D^{'N-1}(g_{cen}))\} \mid p = 1,2,...,P \quad (5)$$

Where

$$f_6(\mathrm{Im}\, g_D^{'N-1}(g_p), \mathrm{Im}\, g_D^{'N-1}(g_{cen})) = \begin{cases} \mathrm{Im}\, g_D^{'N-1}(g_p), & if \ \ \mathrm{Im}\, g_D^{'N-1}(g_{cen}) \\ 0 & \text{else} \end{cases} \quad (6)$$

From Equations (5) and (6) we computed the T-LOP code as given in Equation (7):

$$TLOP_P^N \mid_{\{\overline{D} \mid \forall D, \exists \neg \mathrm{Im}\, g_D^{'N-1}(g_{cen})\}} = f_7(TLOP_P^N(g_{cen})) \mid_{\{\overline{D} \mid \forall D, \exists \neg \mathrm{Im}\, g_D^{'N-1}(g_{cen})\}} \quad (7)$$

The remaining 7 T-LOP patterns are computed from Equation (8) as:

$$f_7(TLOP_D^N(g_{cen})) \mid_{\overline{D} \in \overline{D}} = \begin{cases} 1, & if \ \ TLOP_D^N(g_{cen}) = \overline{D} \\ 0 & else \end{cases} \quad (8)$$

Here, $\overline{D}$ represents the quadrants except for the referenced pixel and $\vec{D}$ is showing the one quadrant from the whole set $\overline{D}$. The final T-LOP code is computed by Equation (9):

$$\begin{aligned}
&TLOP_P^N \mid_{\{\overline{D} \mid \forall D, \exists \neg \mathrm{Im}\, g_D^{'N-1}(g_{cen})\}} = \\
&\sum_{p-1}^{P} 2^{(p-1)} * f_7(TLOP_P^N(g_{cen})) \mid_{\{\overline{D} \mid \forall D, \exists \neg \mathrm{Im}\, g_D^{'N-1}(g_{cen})\}}
\end{aligned} \quad (9)$$

And the Magnitude Pattern (MP) is computed by Equation (10):

$$MP = \sum_{p=1}^{P} 2^{N-1} * f_8(M_{\mathrm{Im}\, g(g_p)} - M_{\mathrm{Im}\, g(g_{cen})}) \quad (10)$$

Where $g_p$ is given by Equation (11):

$$M_{\mathrm{Im}\, g(g_p)} = \sqrt{\sum \begin{pmatrix} (\mathrm{Im}\, g_{0^\circ}^{'N-1}(g_p))^2 + (\mathrm{Im}\, g_{45^\circ}^{'N-1}(g_p))^2 + \\ (\mathrm{Im}\, g_{90^\circ}^{'N-1}(g_p))^2 + (\mathrm{Im}\, g_{135^\circ}^{'N-1}(g_p))^2 \end{pmatrix}} \quad (11)$$

- *Glaucoma classification using SVM classifier*: in this step, the computed features are used to train the SVM classifier to categories the input sample into respective classes i.e., healthy, glaucomatous. The reason to choose the SVM classifier as compared to other techniques is because of its ability to cope with the problem of high dimensional space [5] and its efficiency to deal with the over-fitted training data. Moreover, SVM minimizes the empirical error and performs well for unknown data.

For given two-class data set $(x, y)_{j=1}^{l}$, SVM draws an optimal hyper-plane to classify the samples into different classes through maximizing the margin $\frac{1}{||w||^2}$ by calculating through Equation (12):

$$\max \frac{1}{||w||^2} \quad (12)$$

Concerning $y_j\left(w^T.x_j + b_0\right) \geq 1$ where j∈ 1, 2, …l decision rule defined as $f$: x–y is given by Equation (13):

$$f(x) = sgn\left(\sum_{j=1}^{l} y_j w_j.x + b_0\right) \quad (13)$$

The twofold form is employed to resolve the problem Equation (14):

$$Max\ W(\alpha) = \sum_{j=1}^{l} \alpha_j - 0.5 * \sum_{j,i=1}^{l} \alpha_j \alpha_i y_j y_i (x_j.x_i) \quad (14)$$

Concerning Equation (15):

$$\sum_{j=1}^{l} \alpha_j y_j = 0, \ \ 0 \leq \alpha_j \leq \frac{c}{l} \ \text{ where j∈ 1,2,…l} \quad (15)$$

The decision rule for the twofold form is given as in Equation (16):

$$f(x) = sgn\left(\sum_{j=1}^{l} y_j \alpha_j a_j.\ x + b_0\right) \quad (16)$$

Here the $x_j$ is showing a support vector. However, for non-linear samples, a mapping function $\phi$: $x - \phi(x)$ is used to plot the data to high dimensional space which SVM computes through Equation (17):

$$Max\ W(\alpha) = \sum_{j=1}^{l} \alpha_j - 0.5 * \sum_{j,i=1}^{l} \alpha_j \alpha_i y_j y_i (\phi(x_j).\phi(x_i)) \quad (17)$$

Concerning:

$$\sum_{j=1}^{l} \alpha_j y_j = 0, \ \ 0 <= \alpha_j <= \frac{c}{l} \ \ \text{where j∈ 1,2,…l}$$

And now the decision function is defined by Equation (18):

$$f(x) = sgn\left(\sum_{j=1}^{l} y_j \alpha_j \phi(x_j).\ \phi(x_j) + b_0\right) \quad (18)$$

As mentioned earlier, the SVM classifier works well in high dimensional space as everything is a dot product, so a kernel function $k(x,x)$ is employed. If the symmetric kernel satisfies Mercer's theorem, then there is the final mapping is given by Equation (19):

$$k(x, \tilde{a}) = \phi(a) - \phi(\tilde{x}) \quad (19)$$

- *Content-based Image Retrieval*: after classifying the input sample using an SVM classifier, we locate the top-query neighborhood from the given set of fundus images with the same class group. The similarity is measured by employing the Euclidean-distance formula. The main objective of determining the top-query neighbors is to support the computed decision for a given case related to prescriptions. Although, in represented work, as we are not able to have the medical history of related fundus images, however, the involvement of this concept is our target for future work.

## 4. Experiments and Results

In this section, we will discuss the dataset and evaluation parameters that we have used to evaluate the performance of our proposed work.

- *Dataset*: To evaluate the glaucoma detection and classification performance of our proposed methodology, we have employed the two publicly available datasets of glaucoma fundus images named HRF [22] and ORIGA [23]. The HRF dataset consists of total 45 images, of which 15 images are of normal eye type, while 15 images are of glaucoma affected category, and the remaining 14 images are Diabetic Retinopathy (DR) affected. While the second dataset named ORIGA contains total 650 images in which 168 are glaucomatous affected images while the remaining 650 are normal eye images. The sample images of both datasets are represented in Figure 3.
- *Evaluation Parameters:* to analyze the classification power of the introduced technique, we have employed several metrics named sensitivity (sen), specificity (spe), accuracy (acc), and area under the curve (auc) defined by Equations (20), (21) and (22) respectively:

$$\text{sen} = \frac{tp}{tp+fn} \tag{20}$$

$$\text{spe} = \frac{tn}{tn+fp} \tag{21}$$

$$\text{acc} = \frac{tp}{tp+fp} \tag{22}$$

Where *tn tp, tn, fp* and *fn* are representing the true positive, true negative, false positive, and false negative cases respectively.

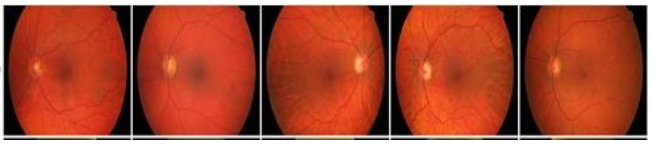

a) HRF dataset.

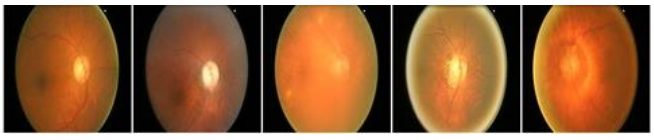

b) ORIGA database.

Figure 3. Sample Images.

- *Results*: the evaluation power of our represented methodology for classifying the glaucoma lesion has been evaluated in this section. We have employed an SVM classifier for glaucoma classification. It can be seen observed from the results that the SVM classifier has efficiently classified the images. Table 1 shows the database wise classification evaluation results of the represented solution in terms of accuracy, sensitivity, specificity, and AUC. For the HRF dataset, our work has attained the average accuracy of 97.2% along with the average values of 0.962 and 0.96 for sensitivity and specificity while for the ORIGA dataset it achieves the 96.7, 0.951, and .0946 values of accuracy, sensitivity, and specificity respectively which are depicting the capability of the introduced technique.

Table 1. Dataset wise performance evaluation of the proposed method.

| Dataset | Acc | Sen | Sp | auc |
|---|---|---|---|---|
| HRF [3] | 97.2% | 0.962 | 0.96 | 0.965 |
| ORIGA [34] | 96.7% | 0.951 | 0.946 | 0.932 |
| **Average** | **96.9%** | **0.956** | **0.953** | **0.948** |

Figure 4 is showing the class-wise performance results of the introduced solution in terms of sensitivity and specificity. Our approach has achieved the average values of .956 and .953 of sensitivity and specificity respectively along with .946 value of AUC which is exhibiting the competitive nature of the proposed framework.

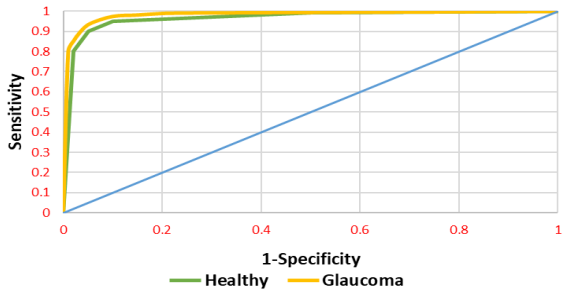


Figure 4. Class wise performance of the proposed methodology.

- *Comparison with state-of-the-art techniques*: in this section, we have compared the results of the presented approach against most related studies from history which employed the same databases for results evaluation. For the HRF dataset, comparison results are reported in Table 2. It can be visualized that our approach achieved 97.2% accuracy and 97% AUC which is highest than all the comparative methods. However, in the case of specificity, the approach in [22] attained a higher value than our framework but this approach is computationally more complex than our method. The introduced framework attained the average AUC of 97 while the comparative approaches achieved the average AUC of 89.06, hence, our method achieved a 7.94% performance gain. Similarly, the specificity value of our method is 93.3 while the average specificity value of comparative approaches is 87.8, which depicts the 5.5% performance gain. In terms of average accuracy, our work achieved 97.2, whereas other approaches showed an average accuracy value of 73.16. Therefore, we can say that our method gave a 24.04% performance gain and more robust to glaucoma lesion classification than the rest of the approaches. For ORIGA database evaluation results are shown in Table 3. From results, one can see clearly that our approach exhibits promising results as compared to other methods as deep networks can easily encounter the problem of over-fitting. As in our technique, the SVM classifier can deal with an over-fitted model, therefore the proposed work has shown state-of-the-art performance.

Table 2. Comparison results with state-of-the-arts over HRF dataset.

| Approach | auc | sp | acc |
|---|---|---|---|
| Xception [6] | 83 | 78 | 80 |
| ResNet-50 [28] | 86 | 79 | 52 |
| GoogLeNet [28] | 85 | 93 | 76 |
| ResNet-152 [28] | 95 | 93 | 62 |
| Nazir *et al*. [22] | 96.3 | 96 | 95.8 |
| **Proposed** | **97** | **93.3** | **97.2** |

Table 3. Comparison with state-of-the-art techniques over ORIGA dataset.

| Technique | auc |
|---|---|
| Cheng *et al*. [4] | 80 |
| *Xu* et al.[32] | 82.3 |
| Navab *et al*. [21] | 83.8 |
| Li *et al*. [14] | 84.83 |
| **Proposed** | **93.2** |

## 5. Conclusions

Early and accurate detection of glaucoma lesion is a challenging task due to its varying texture, shape, complex screening process and high computational complexity. The manual localization of the glaucoma lesion needs experienced human resources to locate the small details from the colored fundus images and classify them into different groups through a complicated grading system. To cope with the challenges of a manual glaucoma detection system, a robust automated technique based on T-LOP pattern features along with an SVM classifier has been introduced in the represented work. We have evaluated our approach over two datasets namely ORIGA and HRF. For the ORIGA dataset, we have attained a 97.2% accuracy value while for HRF we obtained 96.7% accuracy value. The reported results show that our method can accurately determine the adversity level of the disease by showing the matching historical cases for an effective prescription. As opposed to other latest glaucoma detection methods, our proposed framework can calculate the discriminative key points from the low intensity and noisy data images and efficiently classify them in their respective classes. Hence this approach can play an important role in automated recognition of glaucoma lesions and can assist the experts to perform their work more efficiently. In the future, we plan to extend our technique to apply it to more complicated glaucoma datasets and to other medical diseases as well.

## References

[1] Bajwa M., Malik M., Siddiqui S., Dengel A., Shafait F., Neumeier W., and Ahmed S., "Two-Stage Framework for Optic Disc Localization and Glaucoma Classification in Retinal Fundus Images Using Deep Learning," *BMC Medical Informatics and Decision Making*, vol. 19, no. 1, pp. 136, 2019.

[2] Bakhsheshi M., Ho M., Keenliside L., and Lee T., "Non-Invasive Monitoring of Brain Temperature During Rapid Selective Brain Cooling by Zero-Heat-Flux Thermometry," *Emerging Science Journal*, vol. 3, no. 1, pp. 1-9, 2019.

[3] Budai A., Bock R., Maier A., Hornegger J., and Michelson G., "Robust Vessel Segmentation in Fundus Images," *International Journal of Biomedical Imaging*, vol. 2013, no. 1, 2013.

[4] Cheng J., Liu J., Xu Y., Yin F., Wong D., Tan N., Tao D., Cheng C., Aung T., and Wong T., "Superpixel Classification Based Optic Disc and Optic Cup Segmentation for Glaucoma Screening," *IEEE Transactions on Medical Imaging*, vol. 32, no. 6, pp. 1019-1032, 2013.

[5] Cortes C. and Vapnik V., "Support-Vector Networks," *Machine Learning*, vol. 20, no. 3, pp. 273-297, 1995.

[6] Diaz-Pinto A., Morales S., Naranjo V., Köhler T., Mossi J., and Navea A., "Cnns for Automatic Glaucoma Assessment Using Fundus Images: An Extensive Validation," *Biomedical Engineering Online*, vol. 18, no. 1, pp. 29, 2019.

[7] Gargeya R. and Leng T., "Automated Identification of Diabetic Retinopathy Using Deep Learning," *Ophthalmology*, vol. 124, no. 7, pp. 962-969, 2017.

[8] Gómez-Valverde J., Antón A., Fatti G., Liefers B., Herranz A., Santos A., Sánchez C., and Ledesma-Carbayo M., "Automatic Glaucoma Classification Using Color Fundus Images Based on Convolutional Neural Networks and Transfer Learning," *Biomedical Optics Express*, vol. 10, no. 2, pp. 892-913, 2019.

[9] Guo J., Azzopardi G., Shi C., Jansonius N., and Petkov N., "Automatic Determination of Vertical Cup-to-Disc Ratio in Retinal Fundus Images for Glaucoma Screening," *IEEE Access*, vol. 7, no. 1, pp. 8527-8541, 2019.

[10] Haddrill M. and Slonim C., "What Causes Glaucoma?," Available from: http://www.allaboutvision.com/conditions/glaucoma-2-cause.htm., Last Visited, 2019.

[11] Hagiwara Y., Koh J., Tan J., Bhandary S., Laude A., Ciaccio E., Tong L., and Acharya U., "Computer-Aided Diagnosis of Glaucoma Using Fundus Images: A Review," *Computer Methods Programs in Biomedicine*, vol. 165, no. 1, pp. 1-12, 2018.

[12] Hemelings R., Elen B., Barbosa-Breda J., Lemmens S., Meire M., Pourjavan S., Vandewalle E., Van de Veire S., Blaschko M., and De Boever P., "Accurate Prediction of Glaucoma from Colour Fundus Images with a Convolutional Neural Network That Relies on Active and Transfer Learning," *Acta Ophthalmologica*, vol. 98, no. 1, pp. e94-e100, 2020.

[13] Kartubi N., Firmansyah A., Pardi P., and Budiantari C., "Preparation for Eye Lens Dose

Assessment at Cstrm-Nnea," *SciMedicine Journal*, vol. 2, no. 1, pp. 30-37, 2020.

[14] Li A., Wang Y., Cheng J., and Liu J., "Combining Multiple Deep Features for Glaucoma Classification," *in Processing of IEEE International Conference on Acoustics, Speech and Signal Processing*, Calgary, pp. 985-989, 2018.

[15] Li F., Yan L., Wang Y., Shi J., Chen H., Zhang X., Jiang M., Wu Z., and Zhou K., "Deep Learning-Based Automated Detection of Glaucomatous Optic Neuropathy on Color Fundus Photographs," *Graefe's Archive for Clinical and Experimental Ophthalmology*, vol. 258, no. 4, pp. 1-17, 2020.

[16] Li L., Xu M., Liu H., Li Y., Wang X., Jiang L., Wang Z., Fan X., and Wang N., "A Large-Scale Database and a Cnn Model for Attention-Based Glaucoma Detection," *IEEE Transactions on Medical Imaging*, vol. 39, no. 2, pp. 413-424, 2019.

[17] Liao W., Zou B., Zhao R., Chen Y., He Z., and Zhou M., "Clinical Interpretable Deep Learning Model for Glaucoma Diagnosis," *IEEE Journal of Biomedical and Health Informatics*, vol. 24, no. 5, pp. 1405-1412, 2019.

[18] Madzin H., Zainuddin R., and Mohamed N., "Analysis of Visual Features in Local Descriptor for Multi-Modality Medical Image," *The International Arab Journal of Information Technology*, vol. 11, no. 5, pp. 468-475, 2014.

[19] Marsden J., "Glaucoma: The Silent Thief of Sight," *Nursing Times*, vol. 110, no. 42, pp. 20-22, 2014.

[20] Martins J., Cardoso J., and Soares F., "Offline Computer-Aided Diagnosis for Glaucoma Detection Using Fundus Images Targeted at Mobile Devices," *Computer Methods and Programs in Biomedicine*, vol. 192, no. 1, pp. 105341, 2020.

[21] Navab N., Hornegger J., Wells W., and Frangi A., *Medical Image Computing and Computer-Assisted Intervention–MICCAI 2015*, Springer, 2015.

[22] Nazir T., Irtaza A., Javed A., Malik H., Hussain D., and Naqvi R., "Retinal Image Analysis for Diabetes-Based Eye Disease Detection Using Deep Learning," *Applied Sciences*, vol. 10, no. 18, pp. 6185, 2020.

[23] Pratt H., Coenen F., Broadbent D., Harding S., and Zheng Y., "Convolutional Neural Networks for Diabetic Retinopathy," Procedia Computer Science, vol. 90, no. 1, pp. 200-205, 2016.

[24] Quellec G., Charrière K., Boudi Y., Cochener B., and Lamard M., "Deep Image Mining for Diabetic Retinopathy Screening," *Medical Image Analysis*, vol. 39, no. 1, pp. 178-193, 2017.

[25] Quigley H. and Broman A., "The Number of People with Glaucoma Worldwide in 2010 and 2020," *British Journal of Ophthalmology*, vol. 90, no. 3, pp. 262-267, 2006.

[26] Quigley H. and Green W., "The Histology of Human Glaucoma Cupping and Optic Nerve Damage: Clinicopathologic Correlation in 21 Eyes," *Ophthalmology*, vol. 86, no. 10, pp. 1803-1827, 1979.

[27] Schoenemann B., "Evolution of Eye Reduction and Loss in Trilobites and Some Related Fossil Arthropods," *Emerging Science Journal*, vol. 2, no. 5, pp. 272-286, 2018.

[28] Serte S. and Serener A., "A Generalized Deep Learning Model for Glaucoma Detection," *in Proceedings of 3rd International Symposium on Multidisciplinary Studies and Innovative Technologies*, Ankara, pp. 1-5, 2019.

[29] Shabbir Z., Irtaza A., Javed A., and Mahmood M., "Tetragonal Local Octa-Pattern (T-Lop) Based Image Retrieval Using Genetically Optimized Support Vector Machines," *Multimedia Tools Applications*, vol. 78, no. 16, pp. 23617-23638, 2019.

[30] Tham Y., Li X., Wong T., Quigley H., Aung T., and Cheng C., "Global Prevalence of Glaucoma and Projections of Glaucoma Burden through 2040: A Systematic Review and Meta-Analysis," *Ophthalmology*, vol. 121, no. 11, pp. 2081-2090, 2014.

[31] Varma R., Lee P., Goldberg I., and Kotak S., "An Assessment of the Health and Economic Burdens of Glaucoma," *American Journal of Ophthalmology*, vol. 152, no. 4, pp. 515-522, 2011.

[32] Xu Y., Lin S., Wong D., Liu J., and Xu D., "Efficient Reconstruction-Based Optic Cup Localization for Glaucoma Screening," *in Proceedings of International Conference on Medical Image Computing and Computer-Assisted Intervention*, Nagoya, pp. 445-452, 2013.

[33] Yu S., Xiao D., Frost S., and Kanagasingam Y., "Robust Optic Disc and Cup Segmentation with Deep Learning for Glaucoma Detection," *Computerized Medical Imaging and Graphics*, vol. 74, pp. 61-71, 2019.

[34] Zhang Z., Yin F., Liu J., Wong W., Tan N., Lee B., Cheng J., and Wong T., "Origa-Light: An Online Retinal Fundus Image Database for Glaucoma Analysis and Research," *in Proceedings of Annual International Conference of the IEEE Engineering in Medicine and Biology*, Buenos Aires, pp. 3065-3068, 2010.

[35] Zhao R., Liao W., Zou B., Chen Z., and Li S., "Weakly-Supervised Simultaneous Evidence Identification and Segmentation for Automated Glaucoma Diagnosis," *in Proceedings of the AAAI Conference on Artificial Intelligence*, Honolulu, pp. 809-816, 2019.

**Marriam Nawaz** completed BSc (Software Engineering) from University of Engineering and Technology, Taxila, and secured Gold Medal. Completed her M.Sc. degree in Software Engineering from University of Engineering and Technology, Taxila, with specialization in Software Engineering Discipline. Currently enrolled in Ph.D. Program in Software Engineering at UET, Taxila. Since 2017, she has been serving as Programmer at Computer Science Department, UET Taxila. Her research interests include Image processing, Medical Image Analysis, Digital Image Forgery detection, and Deep-fakes Detection.

**Tahira Nazir** currently working toward the Ph.D. degree at Department of Computer Science in University of Engineering and Technology, Taxila, Pakistan. She has done the MS(CS) from Department of Computer Science, UET Taxila, Pakistan in 2016. Her research interests are Computer Vision, Medical Imaging, Machine Learning and Data Science etc.

**Momina Masood** since 2017 working as a Programmer at University of Engineering and Technology, Taxila, Pakistan. She received the MS degree in computer science in 2018 and currently, she is a Ph.D. candidate at Department of Computer Science in University of Engineering and Technology, Taxila, Pakistan. Her current research interests include Computer Vision, Machine Learning, and Medical Imaging.